Materials Today Communications 28 (2021) 102512. Doi: https://doi.org/10.1016/j.mtcomm.2021.102512

Suppression of the surface roughness and fluctuation frequency by electric method

R. S. Qin

School of Engineering & Innovation, The Open University, Milton Keynes MK7 6AA, England

Corresponding author: R.S. Qin: Tel: +44 1908 652 999 Email: rq282@open.ac.uk

ABSTRACT

The descriptions of materials surface geometry by noise theory and metrological method have been compared. An equation to reproduce the roughness and fluctuation frequency is suggested to model the surface. Numerical calculation shows that the surface area is dependent not only on the roughness but also the fluctuation behaviour. Using Boltzmann distribution to describe the forming possibility of various surface geometries enables to link possibility to system free energy. Through the numerical calculation of electric free energy, it is fount that electric field possess a significant retardation effect to the amplitude and frequency of surface fluctuation. The critical value of electric potential gradient to generate an electric effect to be comparable to surface energy is typically around 1 volt/cm, which is achievable in engineering practise. Further calculation shows that the critical values for various liquid iron surfaces are between 2.27 and 4.10 volts/cm and that for liquid aluminium are between 0.26 and 0.47 volts/cm. The reduced surface fluctuation curvature and surface area contribute to lubrication, corrosion resistance, crack initiation and wear resistance of materials.

Keywords: Roughness, Boltzmann distribution, Electric free energy, wavelets

1. INTRODUCTION

Surface roughness affects interaction between materials that approach or contact to each other [1-2]. The non-contact interaction consists of van der Waals force and electrostatic force, as is described by DLVO theory developed by Derjaguin, Landau, Verwey and Overbeek [3]. The interaction can be measured using atomic force microscope [4-5]. Surface roughness affects the effective distance between objects and hence influences the distribution of electrostatic field around the materials surface. The interaction between contacted materials is due to elastic deformation. The distribution of elastic strain is affected by the surface roughness and surface fluctuation frequencies [6-7].

Processing of materials to improve materials surface properties are widely seen from research laboratory to engineering application [8-10]. Roughness and surface fluctuation behaviour affects materials adhesion, lubrication, crack initiation, corrosion and diffraction of electromagnetic waves [11-12]. Surface geometry can be affected by many factors such as environmental perturbation, phase transition, stress evolution, fluid convection and intrinsic fluctuation during materials processing, e. g. in casting and solidification. Some factors can be controlled by improving the materials processing conditions. However, there is no method so far to expediate surface evolution from rough to smooth states. Moreover, the mechanical treatment (such as rolling and polishing) is the usual way to improve the materials surface quality during or post the materials fabrication. This is, however, only applicable to the outward surface that can be physically reachable. Many inward surfaces, such as the sealing chambers and bolt holes in machine tools, are not reachable. Those surfaces contain many burrs that affect the sealing and cause leaking, fall into the chamber and cause pollution, create gap between contacting parts and demote precision. There is so far no method to be able to improve the surface quality in such situation. The research in this work aims to invent such mechanism.

Experimental observation on the retardation of materials surface roughness has been reported on several occasions where pulse electric current was implemented in the processing. Examples include a significant reduction of surface roughness for pure titanium [13] and Ti-6Al-4V alloy [14] in electropulsing-assisted ultrasonic surface processing. These experiments

demonstrated that electropulsing played an important role in the modification of surface properties for metals and alloys. However, it is not clear how the electropulsing affects the reconstruction of surface geometry because several phenomena (e. g. recrystallization and electroplasticity) take places simultaneously. To identify the fundamental mechanisms behind the electropulsing-induced surface modification, this research simplifies the processing system to an ideal case, i.e., applying electric field to an isothermal conductive molten material. The approximation allows to neglect the effects of microstructural transformation, stress redistribution and convection on the formation and evolution of surface geometry. The theoretical approximation is described in section 2. Section 3 presents the numerical calculations based on some realistic materials and processing parameters. The numerical results are discussed in section 4. The conclusions are presented in section 5.

2. MODELLING AND THEORY

Surface roughness of a material is measured by the derivations of real surface in the direction of the normal vector from its assumed smooth form. Although a rough surface can be approximated as two-dimensional random noise [15], surface metrology typically considers it to be a high frequency short-wavelength texture. In practice, it is often necessary to know both the amplitude and frequency of fluctuation in order to ensure the surface properties being suitable for engineering requirement [8]. There are several definitions for the surface roughness. The most widely used one is called R_a value, which is defined as the arithmetical mean deviation of the surface profile as following [16].

$$R_a = \frac{1}{l_\alpha} \int^{l_\alpha} |y_r(x,z) - y_s(x,z)|\, dl \tag{1}$$

where l_α is the surface profile, y_r is the local height at rough surface and y_s is the corresponding hight at smooth state. According to perturbation theory, the surface of a material will take one of the possible shapes with a statistical possibility. The latter obeys following Boltzmann distribution [17].

$$P_r = P_s \exp\left(-\frac{E_r - E_s}{kT}\right) \tag{2}$$

where P_r is the possibility to form a rough surface. P_s is the possibility to form a smooth surface, E_r and E_s are the system free energy of a material with rough and smooth surfaces, respectively. k is Boltzmann's constant. T is temperature. When the dimension of E_r and E_s is molar energy, k should be replaced by the gas constant R. Boltzmann distribution can be obtained from either the microcanonical derivation or the maximum entropy principal derivation [18]. The system free energy generally consists of chemical free energy, strain-stress energy, surface energy and external field free energy. For a liquid homogeneous material at isothermal condition and without phase transition to take place, the chemical free energy is independent of surface geometry as it depends only on the chemical composition and fraction of each phase. The residual stress in liquid can be quickly relaxed via flowing. Therefore, the difference of system free energy between two surface states is reduced to consist only the change of surface energy and electric free energy.

$$\Delta G_{rs} = E_r - E_s = (E_r^{sur} - E_s^{sur}) + \left(E_r^{elec} - E_s^{elec}\right) = \Delta E^{sur} + \Delta E^{elec} \tag{3}$$

where E_r^{sur} and E_s^{sur} are surface energy of rough surface and smooth surface, G_r^{elec} and G_0^{elec} the electric free energy of systems with rough and smooth surfaces, and $\Delta E^{sur} = E_r^{sur} - E_s^{sur}$ and $\Delta E^{elec} = E_r^{elec} - E_s^{elec}$ the change of surface energy and electric free energy, respectively. ΔE^{sur} can be obtained from the surface tension (σ) and surface area (S_r and S_s) via the following equation. The approximation has neglected the curvature-dependent surface tension (surface moment) [19].

$$\Delta E^{sur} = \sigma(S_r - S_s) \tag{4}$$

Application of electric field to conductive material generates electric current. The electric free energy for a material carrying electric current is defined by Landau theory as [20]

$$E_r^{elec} = -\frac{1}{2}\int\left(\vec{H}_r \cdot \vec{B}_r\right)dv \tag{5}$$

where $\vec{H}_r$ is the magnetic field strength and $\vec{B}_r$ is the magnetic field of the system with a rough surface. The integration goes throughout the space. It should be emphasised that Eq. (5) lists only one of five terms in the original Landau theory. The rest four terms have three terms applicable only to multiferroic and magnetoelectric materials and another term applicable to

non-conductive materials. A priori derivation of Eq. (5) has been published previously [21]. Due to slow convergence of magnetic field, the integration in Eq. (5) requires covering a volume far large than that of the material. This can only be done by analytical derivation for a few very simple geometries [22]. Using the electromagnetic equations $\vec{B}_r = \nabla \times \vec{A}_r$ and $\nabla \times \vec{H}_r = \vec{j}_r$, the vector calculation equation $\vec{H}_r \cdot (\nabla \times \vec{A}_r) = \vec{A}_r \cdot (\nabla \times \vec{H}_r) - \nabla \cdot (\vec{H}_r \times \vec{A}_r)$ and the divergence theorem , Eq. (5) can be converted to its equivalent format as [21]

$$E_r^{elec} = -\frac{1}{2}\int (\vec{A}_r \cdot \vec{j}_r) dv \tag{6}$$

where $\vec{A}_r$ is the vector potential and $\vec{j}_r$ the electric current density. The integration in Eq. (6) only goes over the volume of conductive material where electric current density is not zero. Further derivation leads to the following format.

$$\Delta E^{elec} = \frac{1}{8\pi}\iint \frac{\mu(v')[\vec{j}_s(v')\cdot\vec{j}_s(v) - \vec{j}_r(v')\cdot\vec{j}_r(v)]}{|v-v'|} dv dv' \tag{7}$$

where $\vec{j}_r(v)$ and $\vec{j}_s(v)$ are electric current density at a space position within an infinitesimal volume v in the materials with rough surface and smooth surface, respectively. μ is the magnetic permeability. Substituting Eqs. (4) and (7) into (3) followed by substituting Eq. (3) to (2), the possibility for the formation of a surface with a given surface geometry can be calculated. If the possibility to form a rough surface is reduced but the possibility to form a smooth surface is increased by the electric method, it indicates that the electric method retards the formation of a rough surface and promotes a smooth surface, and vice versa. From entropy point of view, a system evolves toward a state with maximum amount of possibility. Changing the system free energy toward a state with larger possibility means the state will be achieved in equilibrium.

3. NUMERICAL CALCULATION AND RESULTS

For computational convenience but without to affect the fundamental understanding of the effect of electric processing on the surface geometric evolution, the material is defined to be rectangular parallelepiped with only the top surface to be varied between different roughness and textures. The other five surfaces are kept smooth, as is demonstrated schematically in Fig. 1(a). The material is with a length *L*, height *H* and depth *D*. The volume of material is kept

constant regardless of the surface geometry. This can be achieved by zero-mean fluctuation of surface profile. Two electrodes with voltage V_L and V_R are attached to the left and right surfaces in electric processing. Electric current passes through the conductive material. The rising of temperature due to Ohm heat is assumed to be negligible. In engineering practise, this assumption can be fulfilled by implementing pulse electric current instead of persistent current. In discrete numerical calculation, the computational system includes the material and some surrounding atmosphere. Atmosphere is nonconductive but fills the convex space left by the rough surfaces. The overall computational system is represented by a rectangular adaptive lattice consisting of three layers, namely the surface area, transitional area and bulk area, as is illustrated in Fig. 1(b). The lattice distance in the rough surface area is defined to be the finest to reduce the computational error in approximating the curved surface with staircases. The lattice in bulk materials is coarse in order to minimize computing cost. The materials properties, e.g. the electrical resistance, at a node of lattice are calculated in an enclosure space formed by six perpendicular bisector planes between the node and its 6 neighbouring nodes, as is demonstrated by the dashed box for a two-dimensional adaptive lattice section in Fig. 1(c). This approximation ensures space filling requirement in the discreate numerical computation.

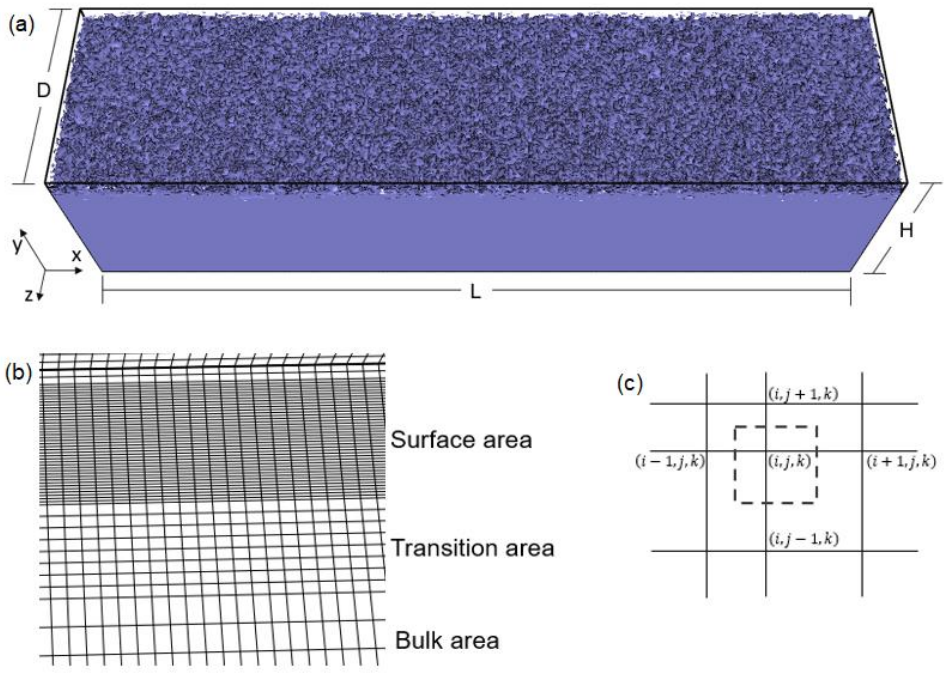

Fig. 1 Schematic diagrams illustrate (a) a material with a top rough surface and five smooth surfaces. The dimensions are in length L, height H and depth D. (b) The adaptive lattice consists of three layers (surface area, transition area and bulk area) to be implemented in numerical calculations. (c) The volume boundaries (dashed lines) to calculate the properties for a node (i, j, k).

3.1 Modelling the surface roughness and fluctuation

Metrology describes a rough surface using high frequency wavelets [8]. While theoretical investigation has frequently modelled the rough surfaces as random noise [1, 15]. In the present work, one compromises both metrological and theoretical approximations and describes a rough surface in Cartesian coordinate by linear combination of the following fluctuation.

$$y_r(x,z) = y_s(x,z) + a_1(1+b\xi)\left\{\sin\left[\left(\frac{n_1 x}{L}+\frac{n_2 z}{D}\right)\pi+\theta_1\right] + a_2\sin\left[\left(n_1\frac{L-x}{L}+\frac{n_2 z}{D}\right)\pi+\theta_2\right]\right\} \quad (8)$$

where a_1 is the primary amplitude parameter. b is the strength of the random fluctuation. ξ is a random number with zero mean and value variated randomly between -0.5 and 0.5. To generator a high-quality random number one has implemented the method developed by Marsaglia et al's [23]. a_2 is the amplitude coefficient for secondary sinusoidal wavelet. n_1 and n_2 are even integers to ensure a constant materials volume. θ_1 and θ_2 are initial angles for the first and second wavelets, respectively. It needs to emphasise that Eq. (8) is one of possible configurations and the real surface is a combination of the equation with corresponding parameters taking different values.

The computation is performed to a material with dimensions at $L = 20\,mm$, $D = 5\,mm$ and $H = 4.5\,mm$. The lattice contains $201 \times 71 \times 51$ nodes. The lattice distance is uniform along *x* and *z* direction but has three adaptive layers along *y* direction: 41 layers in the surface area, 10 layers in transitional area and 20 layers in bulk area. Fig. 2 illustrates four typical numerical calculated surfaces using Eq. (8), where the parameters in 2(a) are $a_1 = 0.1$, $b = 0$, $a_2 = 0$, $n_1 = 24$, $n_2 = 6$; 2(b): $a_1 = 0.5$, $b = 0$, $a_2 = 1$, $n_1 = 24$, $n_2 = 6$; 2(c): $a_1 = 0.5$, $b = 3$, $a_2 = 0.5$, $n_1 = 24$, $n_2 = 6$; and 2(d) $a_1 = 0.5$, $b = 4$, $a_2 = 0.5$, $n_1 = 24$, $n_2 = 6$. The data was plotted using

visualization software MatVisual. It is shown from Fig. 2 that that Eq. (8) is more noise dominated when $b/a > 1$ and b/a goes larger. The surface is more wavelet dominated when b/a is less than 1 and approaches to zero. Fig. 2 shows that Eq. (8) can recover the characteristics of surface geometry in both metrological and theoretical descriptions. The roughness of the surfaces shown in Fig. 2 was calculated using Eq. (1) as: (a) 63.6 μm, (b) 79.6 μm, (c) 85.5 μm and (d) 98.7 μm.

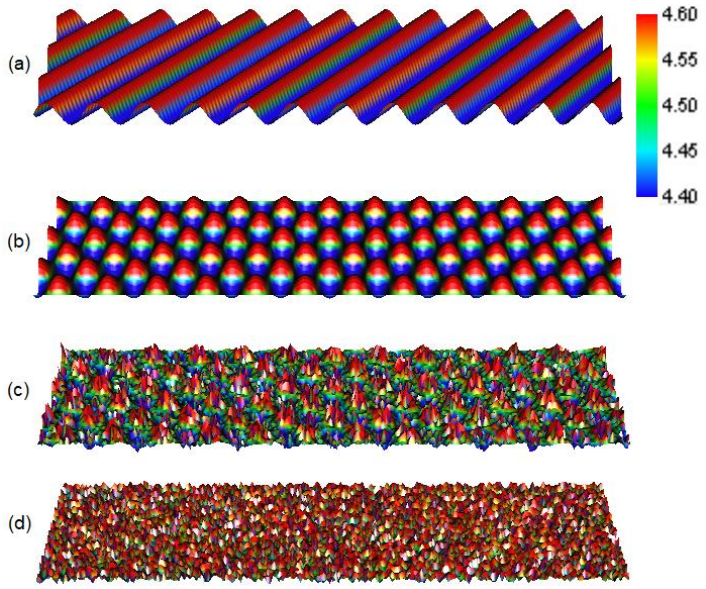

Fig. 2. Surface texture obtained from Eq. (8) with parameters at (a): $a_1 = 0.1$, $b = 0$, $a_2 = 0$, $n_1 = 24$, $n_2 = 6$; (b): $a_1 = 0.5$, $b = 0$, $a_2 = 1$, $n_1 = 24$, $n_2 = 6$; (c): $a_1 = 0.5$, $b = 3$, $a_2 = 0.5$, $n_1 = 24$, $n_2 = 6$; and (d) $a_1 = 0.5$, $b = 4$, $a_2 = 0.5$, $n_1 = 24$, $n_2 = 6$. Their roughness is: (a) 63.6 μm, (b) 79.6 μm, (c) 85.5 μm and (d) 98.7 μm.

According to Eq. (1), the roughness of a surface is dependent on the amplitude parameters a_1 and b but independent of the frequency parameters n_1 and n_2. This can be proved analytically by following derivation.

$$\frac{1}{L}\int_0^L \left| a_1 sin\left(\frac{n\pi}{L}x\right)\right| dx = \frac{2a_1}{\pi}\int_0^{\frac{\pi}{2}} sin\theta d\theta = \frac{2a_1}{\pi} \tag{9}$$

where L is a one-dimensional profile. Eq. (9) indicates that roughness has nothing to do with the frequencies of wavelet.

To demonstrate the effect of wavelet's frequency on surface area, Fig. 3 plots the change of surface area versus various combinations of (n_1, n_2) including (8, 2), (16, 4), (24, 6), (32, 8) and (40, 10) with $a_2 = 0 \; or \; 1$, $b = 0$ and a_1 at various values. It shows clearly that the surface area depends on the wavelet's frequency. Larger frequency causes bigger increase of surface area from the smooth state. This increases the materials surface energy and hence changes their possibility to form such surface geometry.

From engineering point of view, different wavelet's frequency corresponds to different curvatures at the valley of sinusoidal fluctuation. Curvature plays an important role in stress localization, crack initiation and pitting corrosion. This is one of the major reasons to describe materials surface using frequency-dependent wavelets in metrology. On the other side, the theoretical description of surface roughness using random noise approximation does not include the effect of frequency. The method introduced in the present work covers both the surface roughness and fluctuation frequency.

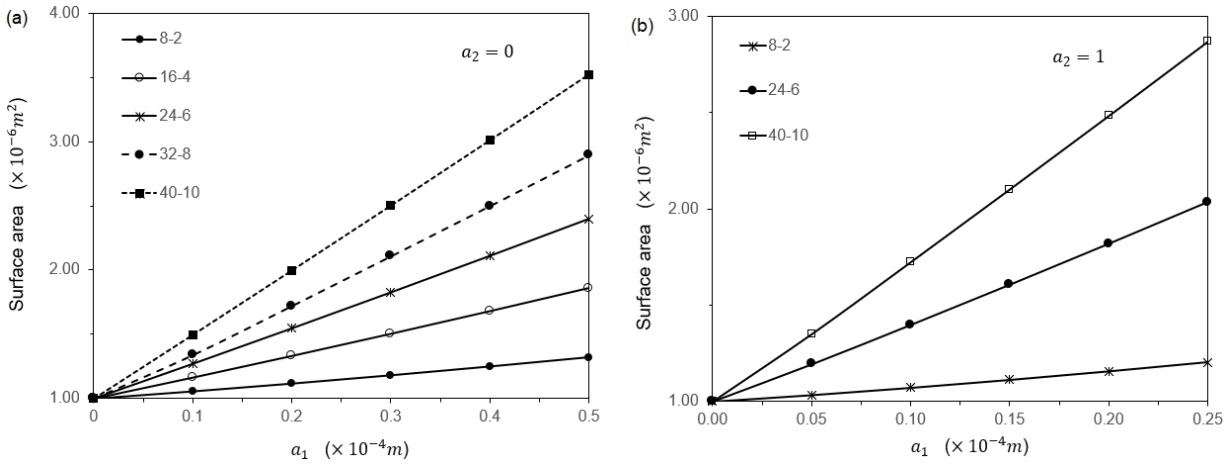

Fig. 3 The relationship between surface area and fluctuation frequency at different values of a_1 and a_2. The values in the legend are n_1 and n_2 in pair. 3(a) is for $\Delta y(x,z) = a_1 \sin\left[\left(\frac{n_1 x}{L} + \frac{n_2 z}{D}\right)\pi\right]$ and 3(b) is for $\Delta y(x,z) = a_1\left\{\sin\left[\left(\frac{n_1 x}{L} + \frac{n_2 z}{D}\right)\pi\right] + \sin\left[\left(n_1 \frac{L-x}{L} + \frac{n_2 z}{D}\right)\pi\right]\right\}$.

3.2 Effect of electric processing on surface evolution

The discrete format of electric free energy is represented as following

$$E_r^{elec} = -\frac{1}{8\pi}\sum_{ijk}\sum_{i'j'k'}\frac{\mu(i,j,k)\vec{j}(i,j,k)\cdot\vec{j}(i',j',k')V(i,j,k)V(i',j',k')}{|r(i,j,k)-r'(i',j',k')|} \quad (10)$$

where (i,j,k) and (i',j',k') represent two different nodes. $V(i,j,k)$ is the volume element of node (i,j,k) to be obtained by the method shown in Fig. 1(c). The electric current between two neighbouring nodes α and β is obtained by Ohm's law as [24]

$$j_{\alpha\beta} = (U_\alpha - U_\beta)\cdot\sigma_{\alpha\beta}/S_{\alpha\beta} \quad (11)$$

where U_α is the electric potential at node α, $\sigma_{\alpha\beta}$ is the electrical conductance between α and β, and $S_{\alpha\beta}$ is the cross-section area between α and β. It is worth to point out that the electrical conductance at a node in adaptive lattice is orientation dependent due to non-uniform lattice distance and non-identical local cross section area between neighbouring nodes. In order to calculate Eq. (10), the distribution of electric current density needs to be calculated firstly. This is achievable by relaxation method, which assume an initial gradient distribution of electric potential across all the nodes and then using time iteration to obtain a static distribution to satisfy the defined boundary conditions. According to Kirchhoff's circuit laws, one obtains the following.

$$U_\alpha(t+1) = \frac{\sum_\beta U_\beta(t)\sigma_{\alpha\beta}}{\sum_\beta \sigma_{\alpha\beta}} \quad (12)$$

where t is the iteration step. The summation goes over all the nearest neighbours. The left and right boundaries are set to the fixed electric potentials V_L and V_R. The zero electric current flux boundary condition is applied to all the lateral surfaces. After each iteration, the total change of electric potential distribution ($\sum_\alpha|U_\alpha(t+1)-U_\alpha(t)|$) is compared with a critical value (δ) to decide whether the relaxation has achieved sufficient accuracy. In the present calculations, the time iteration has been gone over 150,000 time-steps and the absolute critical values are found to be smaller than 10^{-8} volts. The calculation is applied to a material with electrical resistivity at 1.0×10^{-7} Ω·m, which is the electrical resistivity of pure iron at ambient conditions. The non-conductive atmosphere is assumed to be with an electrical resistivity at 6 orders of magnitude higher than that in materials. The magnetic permeability is assigned to be $\mu = 1.25663706\times10^{-6}$ H/m. Using $V_L = 20$ volts and right at $V_R = 0$, the numerical results for electric free energy under various surface textures are calculated and presented in Fig. 4.

The selection of computational parameters was informed by the following experimental facts. Many previous electropulsing experiments on steels microstructure modification utilized AV-108F-2-B-P pulse generator that was powered by a D.C. power at 24 volts [25]. The samples are typically in a few centimetres long and less than 1cm^2 cross section area. The electrical conductivity was selected as iron in ambient temperature to be comparable to the pulsating steel experiments [26].

Fig. 4 shows clearly that the electric free energy increases monotonically with both the primary amplitude of perturbation a_1 and the frequencies of wavelets n_1 and n_2. As is discussed earlier in this work and shown in Eq. (9), the surface roughness R_a is proportional to the amplitude of perturbation a_1. According to Eq. (2), the higher free energy means less possibility to form the corresponding surface texture. According to the second law of thermodynamics, a system intends to evolve from a state with higher free energy to that of a lower one. This indicates that a surface geometry will be driven to evolve from a higher roughness and high fluctuation frequency to lower ones by the applied electric field.

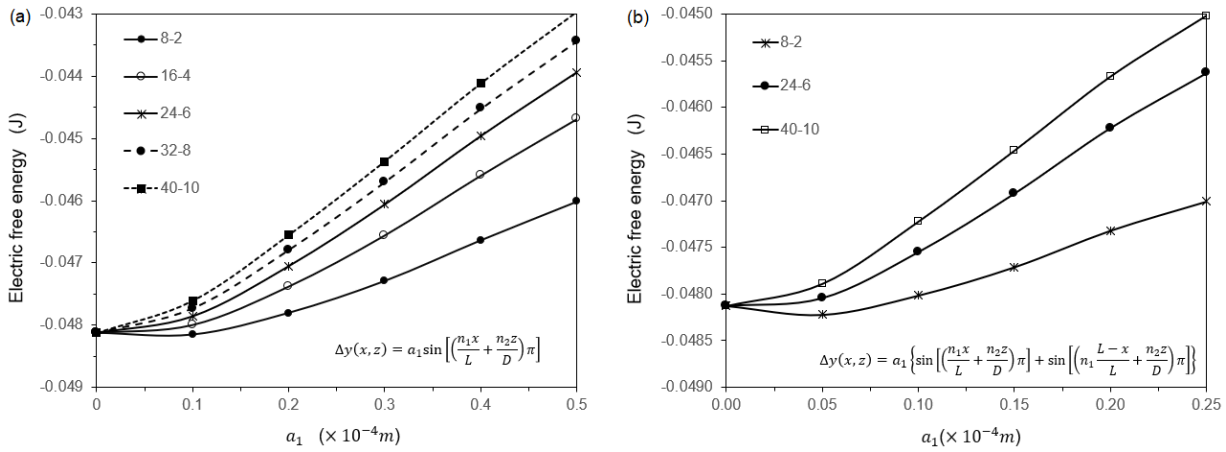

Fig. 4 Change of electric free energy vs a_1, n_1 and n_2 for a surface described by (a) $\Delta y(x,z) = a_1 \sin\left[\left(\frac{n_1 x}{L} + \frac{n_2 z}{D}\right)\pi\right]$ and (b) $\Delta y(x,z) = a_1\left\{\sin\left[\left(\frac{n_1 x}{L} + \frac{n_2 z}{D}\right)\pi\right] + \sin\left[\left(n_1 \frac{L-x}{L} + \frac{n_2 z}{D}\right)\pi\right]\right\}$, where the legend shows the values of n_1 and n_2.

4. DISCUSSION

To demonstrate the intensity of the effect of electric method on the evolution of surface geometry, the change of electric free energy ΔE^{elec} has been compared to the change of surface energy ΔE^{sur} in the same surface geometric evolution. For a liquid with surface tension at 1.61 N/m, which is the measured value for liquid carbon-steel at melting temperature [27], the change of surface area in Fig. 3(a) for case 8-2 is $0.3176 \times 10^{-6}\ m^2$ when a_1 is changed from smooth state at $a_1 = 0$ to rough state at $a_1 = 0.05$ mm. It gives $\Delta E^{sur} = 0.51 \times 10^{-6}\ J$. In the same situation Fig. 4(a) gives $\Delta E^{elec} = 2.1 \times 10^{-3}\ J$. The change of electric free energy has overtaken that of the surface energy considerably. Without electric field the surface evolution from a rough state to smooth state and from a high fluctuation frequency state to low frequency state is driven by the surface energy minimization. This agrees with the numerical results shown in Fig. 3 that a rougher surface has larger surface area than the smooth one and a higher fluctuated surface has larger surface area than that of a lower one. With electric field, however, the driving force for surface evolution is not only from the surface energy minimization but also the electric free energy minimization. Comparation between Fig. 4 and Fig. 3 reveals that the electric field can provide much stronger driving force than that of the surface energy when the electric potential is high enough. The electric field can drive a rough and a strongly fluctuated surface to evolve quicker to its smooth state than via only the surface energy minimization. This allows the surface to achieve closer to its equilibrium smooth state before the temperature drops down and the surface geometry is frozen to the non-equilibrium rough state in materials processing.

The electric free energy depends on the applied electric potential as $G_r^{elec} \propto \left(U_\alpha - U_\beta\right)^2$. To generate the same effect as that of the surface energy, the required electric potential difference is calculated to be 0.31 volts, which is equivalent to a gradient of 0.155 volts/cm and can be achieved easily in engineering practice. If one defines a critical electric processing parameter (V_c) as the electric effect to be equivalent to the effect of surface energy, $\Delta E^{elec}(V_c) = \Delta E^{sur}$, the critical values for other materials can be obtained from the data provided in Figs. 3 and 4. The procedure to determine the critical value include to find out the materials surface tension and

then use the change of surface area in Fig. 3 to obtain the surface energy, and then find out the electrical conductivity of the materials and substitute it to $G_r^{elec} \propto \left[\left(U_\alpha - U_\beta\right)\sigma_{\alpha\beta}\right]^2$ to determine the critical electric potential according to the data provided in Fig. 4. Table 1 presents the results for liquid iron and liquid aluminium using the early mentions procedure.

Table 1. The physical and critical electric processing parameters of liquid iron and aluminium.

Parameter		Liquid iron	Liquid aluminium
Temperature		1823 K	950 K
Electrical resistivity		1.39×10-6 Ω·m [28]	2.29×10-7 Ω·m [29]
Surface tension		1.780 N/m [30]	0.82727 N/m [29]
Surface state and its critical electric processing parameter	8-2	2.27 volts/cm	0.26 volts/cm
	16-4	2.93 volts/cm	0.34 volts/cm
	24-6	3.39 volts/cm	0.39 volts/cm
	32-8	3.73 volts/cm	0.43 volts/cm
	40-10	4.10 volts/cm	0.47 volts/cm

Using the parameters in Table 1, the critical average electric current density for liquid iron is calculated to be 2.94×10^8 A/m^2. This is around the peak electric current density implemented in the reported electropulsing-assisted ultrasonic surface processing of pure titanium [13] and Ti-6Al-4V alloy [14]. Most recently, an alternating magnetic field treatment was found to induce surface roughness modification for nickel-aluminium bronze and aluminium alloy [31], which was believed due to alternating magnetic field-induced eddy current. The numerical results in the current paper provides indication for the mechanism. Experiments have been designed to follow the proposed method in the present work to improve the surface properties of casts. Surface roughness have been reduced by more than 50% in all electropulsed samples. Detailed experiments will be published in another paper.

According to Eq. (2), the surface with higher roughness has less possibilities to form due to the higher surface area-associated surface energy. Fig. 4 indicates the higher electric free energy for the higher roughness and higher frequency wavelets surface. Therefore, the electric

processing will cause smaller possibility to form the surface of higher roughness and higher wavelets' frequency. The change of the formation possibility can be easily calculated by substituting the electric free energy to Eq. (2). This proves that the electric processing suppresses the formation of rough surface and tend to reduce the fluctuation frequency of the surface. Electropulsing helps to fabricate smoother materials surface.

Once the surface wavelets are formed due to perturbation, the linear response theory describes the dissipation of the perturbation as

$$a_1(t) = a_1(0)\exp\left(-\frac{\lambda}{d}t\right) \tag{13}$$

where t is time, λ is viscosity, and d is the mass density of liquid material. The peak of perturbation will be reduced and eventually dissipated. With consideration of surface energy and electric free energy change, an equivalent configuration force will be applied to the surface evolution. The equivalent force is [32]

$$F_e = -\frac{\delta E_r}{\delta a_1} = -\frac{\delta E_r^{sur} + \delta G_r^{elec}}{\delta a_1} \tag{14}$$

The force drives the high free energy surface to move toward the low free energy surface, which accelerates the dissipation of the surface fluctuation. The electric processing also promotes the evolution of the surface from higher frequency wavelets shape to a lower one in order to minimize the electric free energy.

The lower frequency wavelets have large curvature at the tips. This reduces stress localization for a material in loading and hence reduces possibility to initialize surface cracks. The lower curvature also reduces solute aggregation according to Gibbs-Thomson effect. For the materials like stainless steel, the segregation of Cr solute will cause pitting corrosion. The reduction of the curvature will enhance the corrosion resistance. The wear resistance is improved when the surface is less rough and with less sharp heaps.

Fig. 5(a) shows the contour lines of electric potential for the system with surface parameters described in Fig. 4(a) with $n_1 = 8$, $n_2 = 2$ and $a_1 = 4\,mm$.The electric potential in the system reduces monotonically from left at V_L to right at V_R. However, there is a clear jump in the gradient of electric potential around the interface between material and atmosphere. Its effect requires

to be considered in future works. In Fig. 5(b), the length of each arrow is proportional to the current density and the direction of each arrow represents the flow direction at the node. In plotting of arrows, the lattice nodes are skipped by 3 numbers in all Cartesian directions. The denser distribution of arrows in the surface zone is due to the smaller lattice distance between nodes. Electric current flows through the rough bumps in materials surface with reduced current density. The distribution of current density is more clearly shown by the contour lines in Fig. 5(c). The valley has highest electric current density. The heterogeneous distribution of electric current disappears in the bulk zone away from the surface. The change of current distribution between different surface geometries contributes to the change of electric free energy.

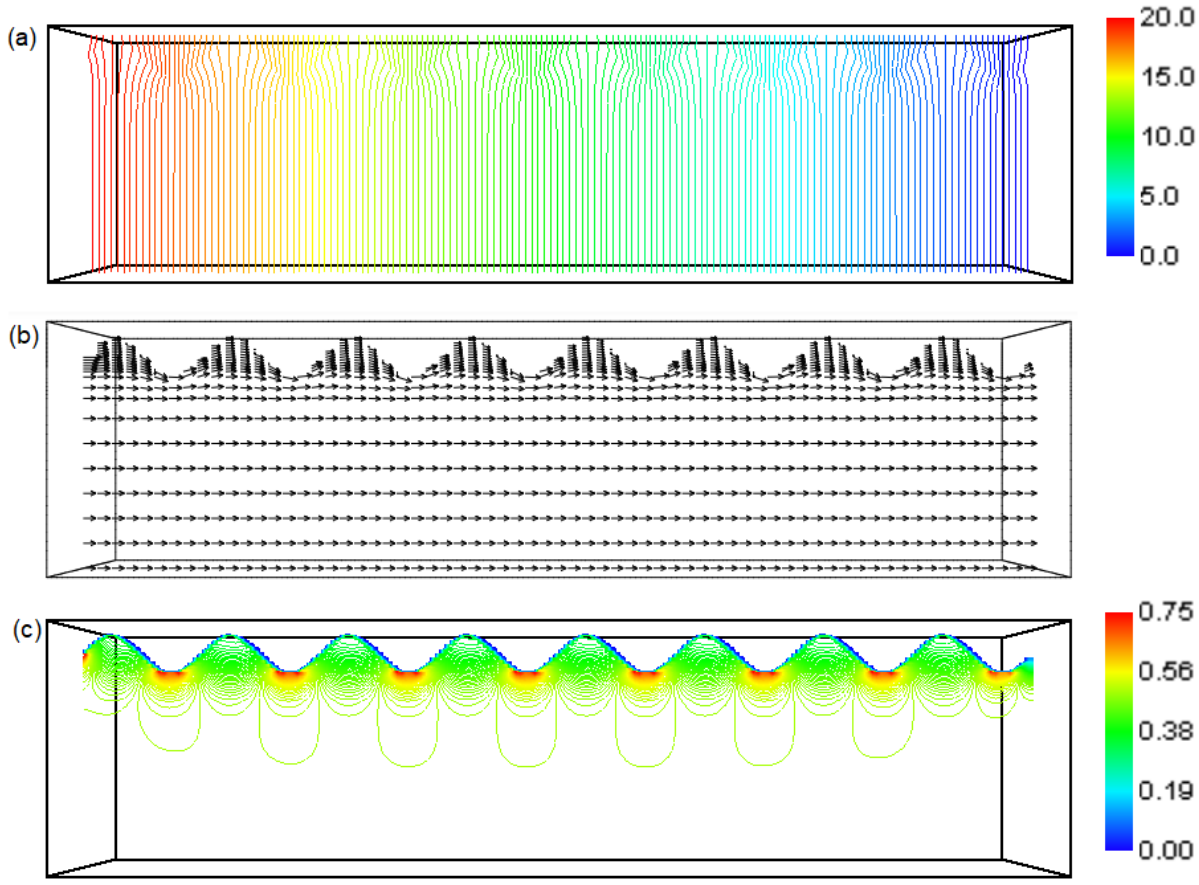

Fig. 5 For the surface profile described by) $\Delta y(x,z) = a_1 \sin\left[\left(\frac{8x}{L} + \frac{2z}{D}\right)\pi\right]$ with $a_1 = 4\,mm$, (a) the contour lines of electric potential, (b) the electric current flow vectors, and (c) the countour of electric current density.

5. CONCLUSIONS AND REMARKS

In summary, an electric method to process surface roughness and fluctuation behaviour for conductive materials has been developed. Followings results have been achieved.

i). The surface geometry of the materials should be described by both the surface roughness and frequency of the perturbation wavelets. The surface roughness is independent of surface fluctuation frequency. However, the frequency is important to the materials properties and performances such as the crack initiation, corrosion and wear rate. The surface geometry can be described by a combination of $y_r(x,z) = y_s(x,z) + a_1(1+b\xi)\left\{\sin\left[\left(\frac{n_1 x}{L}+\frac{n_2 z}{D}\right)\pi+\theta_1\right]+ a_2\sin\left[\left(n_1\frac{L-x}{L}+\frac{n_2 z}{D}\right)\pi+\theta_2\right]\right\}$ with various parameters.

ii). The surface roughness and wavelets' frequency can be modified using electric method. The critical value for generate significant effect of electric effect is from 0.26 volts/cm for liquid aluminium to 4.1 volts/cm for liquid iron for various surface geometries. The effect of electric method on various materials can be obtained using the diagrams reported in the present work. The required parameters are achievable in engineering practise.

iii). The formation of various surface geometries can be calculated by Boltzmann distribution. Both the surface energy and electric free energy affects the formation of surface properties.

iv). The electric method accelerates the kinetic transformation of a rough surface toward the smooth state. The effect is proportional to the square of the applied electric potential.

DATA AVAILABLE ON REQUEST FROM THE AUTHORS: The data that support the findings of this study are available from the corresponding author upon reasonable request.

COMPETING INTERESTS: The author declares no competing interests.

ACKNOWLEDGEMENTS

The author is grateful for the financial support from European Commission RFCS (No. 847269) and EPSRC (No. EP/R029598/1).

REFERENCES

1. D. F. Parsons, R. B. Walsh, and V. S. J. Craig, "Surface forces: Surface roughness in theory and experiment", J. Chem. Phys. **140**, 164701 (2014).
2. C. Kurzthaler, L.L Zhu, A. A. Pahlavan, and H. A. Stone, “Particle motion nearby rough surfaces,” Phys. Rev. Fluids, **5**, 082101(R) (2020).
3. B. Derjaguin and L. Landau, "Theory of the stability of strongly charged lyophobic sols and of the adhesion of strongly charged particles in solutions of electrolytes," Prog. Surf. Sci. **43**, 30-59 (1993).
4. W. A. Ducker, T. J. Senden, and R. M. Pashley, Direct measurement of colloidal forces using an atomic force microscope, Nature, **353**, 239, (1991).
5. M. Elzbieciak-Wodka, M. N. Popescu, F. J. M. Ruiz-Cabello, G. Trefalt, P. Maroni, and M. Borkovec, "Measurements of dispersion forces between colloidal latex particles with the atomic force microscope and comparison with Lifshitz theory" J. Chem. Phys. **140**, 104906 (2014).
6. K. L. Johnson, K. Kendall, and A. D. Roberts, "Surface energy and the contact of elastic solids," Proc. R. Soc. London, Ser. A 324, 301 (1971).
7. B. Derjaguin, V. Muller, and Y. Toporov, "Effect of contact deformations on the adhesion of particles" J. Colloid Interface Sci. 53, 314-326 (1975).
8. P.G. Benardos, G.-C. Vosniakos, "Predicting surface roughness in machining: a review," Int. J. Mach. Tool. Manu. 43, 833–844 (2003).
9. B. N. J. Persson, “Contact mechanics for randomly rough surfaces,” Surf. Sci. Rep. **61**, 201–227 (2006).
10. J. F. Luo and D. A. Dornfeld, "Material removal mechanism in chemical mechanical polishing: Theory and modeling," IEEE Trans. Semicond. Manuf. **14**, 112-133 (2001).
11. Y.F. Mo, K. T. Turner, and I. Szlufarska, "Friction laws at the nanoscale", Nature, **457**, 1116 (2009).

12. R. Kant, "Can current transients be affected by the morphology of the nonfractal electrode?", Phys. Rev. Lett. **70**, 4094-4097 (1993).
13. Y. D. Ye, S. Z. Kure-Chu, Z. Y. Sun, X. P. Li, H.B. Wang, and G.Y. Tang, “Nanocrystallization and enhanced surface mechanical properties of commercial pure titanium by electropulsing-assisted ultrasonic surface rolling," Mater. and Des. **149**, 214-227 (2018).
14. Y. D. Ye, H. B. Wang, G.Y. Tang, G. L. Song, “Effect of electropulsing-assisted ultrasonic nanocrystalline surface modification on the surface mechanical properties and microstructure of Ti-6Al-4V alloy,” J. Mater. Eng. Perform. **27**, 2394-2403 (2018).
15. J. A. Greenwood, "A unified theory of surface roughness," Proc. R. Soc. Lond. A **393**, 133-157 (1984).
16. D. J. Whitehouse, Surfaces and their measurement, first ed. Hermes Penton Ltd, London, 2002.
17. L.D. Landau, E.M. Lifshitz, Statistical physics, Vol.5 third ed. Pergamon Press, Oxford, 1980.
18. X. Gao, E. Gallicchio, and A. E. Roitberg "The generalized Boltzmann distribution is the only distribution in which the Gibbs-Shannon entropy equals the thermodynamic entropy," J. Chem. Phys. **151**, 034113 (2019).
19. X. Gao, Z. P. Huang, and D. N. Fang, "Curvature-dependent interfacial energy and its effects on the elastic properties of nanomaterials", Int. J. Solids Struct., **113–114**, 100-107 (2017).
20. W. Eerenstein, N. D. Mathur & J. F. Scott, "Multiferroic and magnetoelectric materials," Nature, **442**, 759-765 (2006).
21. R.S. Qin, and A. Bhowmik, “Computational thermodynamics in electric current metallurgy,” Mater. Sci. Technol. **31**, 1560-1563 (2015).
22. R.S. Qin, and S.X. Su, “Thermodynamics of crack healing under electropulsing,” J. Mater. Res. **17**, 2048-2052 (2002).
23. G. Marsaglia, A. Zaman, and W. Tsang, “Toward a universal random number generator,” Stat. Probab. Lett. **8**, 35--39 (1990).
24. R.A. Millikan, E.S. Bishop, Elements of Electricity. American Technical Society, (1917).

25. R. S. Qin, A. Rahnama, W. J. Lu, X. F. Zhang, and B. Elliott-Bowman, “Electropulsed steels”, Mater. Sci. Technol. **30**, 1040–1044 (2014).
26. R. S. Qin, E. I. Samuel and A. Bhowmik, “Electropulse-induced cementite nanoparticle formation in deformed pearlitic steels,” J. Mater. Sci. 46, 2838–2842 (2011).
27. I. Egry, E. Ricci, R. Novakovic, S. Ozawa, “Surface tension of liquid metals and alloys - Recent developments,” Adv. Colloid Interface. Sci. **159** ,198–212 (2010).
28. R.W. Powell, “LXXX. The electrical resistivity of liquid iron,” London Edinburgh Philos. Mag. J. Sci., **44**, 772-775 (1953).
29. M. Leitner, T. Leitner, A. Schmon, K. Aziz, and G. Pottlacher, “Thermophysical properties of liquid aluminum,” Metall. Mater. Trans. **48A**, 3036-3045 (2017).
30. M.E. Fraser, W.K. Lu, A. E. Hamielec, and R. Murarka, “Surface tension measurements on pure liquid iron and nickel by an oscillating drop technique,” Metall. Trans. **2**, 817–823 (1971).
31. S. Akram, A. Babutskyi, A. Chrysanthou, D. Montalvão, M. J. Whiting, N. Pizurova, Improvement of the wear resistance of nickel-aluminium bronze and 2014-T6 aluminium alloy by application of alternating magnetic field treatment, Wear, 480–481 (2021) 203940.
32. X.F. Zhang, and R.S. Qin, “Electric current-driven migration of electrically neutral particles in liquids”, Appl. Phys. Lett., **104**, 114106 (2014).